

Structural mediation of human brain activity revealed by white-matter interpolation of fMRI

Anjali Tarun^{a,b,*}, Hamid Behjat^c, Thomas Bolton^{a,b}, David Abramian^{d,e}, Dimitri Van De Ville^{a,b}

^a Institute of Bioengineering, École Polytechnique Fédérale de Lausanne, Geneva, 1202, Switzerland

^b Department of Radiology and Medical Informatics, University of Geneva, Geneva, 1202, Switzerland

^c Center for Medical Image Science and Visualization, University of Linköping, Linköping, 58183, Sweden

^d Department of Biomedical Engineering, University of Linköping, Linköping, 58183, Sweden

^e Department of Biomedical Engineering, Lund University, Lund, 22100, Sweden

ABSTRACT

Understanding how the anatomy of the human brain constrains and influences the formation of large-scale functional networks remains a fundamental question in neuroscience. Here, given measured brain activity in gray matter, we interpolate these functional signals into the white matter on a structurally-informed high-resolution voxel-level brain grid. The interpolated volumes reflect the underlying anatomical information, revealing white matter structures that mediate the interaction between temporally coherent gray matter regions. Functional connectivity analyses of the interpolated volumes reveal an enriched picture of the default mode network (DMN) and its subcomponents, including the different white matter bundles that are implicated in their formation, thus extending currently known spatial patterns that are limited within the gray matter only. These subcomponents have distinct structure-function patterns, each of which are differentially observed during tasks, demonstrating plausible structural mechanisms for functional switching between task-positive and -negative components. This work opens new avenues for the integration of brain structure and function, and demonstrates the collective mediation of white matter pathways across short and long-distance functional connections.

1. Introduction

The coordination of distant neuronal populations gives rise to a vast repertoire of functional networks that underpin human brain function. Using functional magnetic resonance imaging (fMRI), temporally coherent activity can be investigated using measures of functional connectivity (FC) (Friston, 1994). On the other hand, inter-regional communication is mediated by the anatomical scaffold which can be conveniently summarized by structural connectivity (SC) extracted from diffusion-weighted MRI (DW-MRI) (Bullmore and Sporns, 2009). Over the past decade, a particular focus has been dedicated to unraveling how the human brain maintains its vast repertoire of FC states despite being constrained by a rigid anatomical substrate. To bridge the gap between SC and FC, several methods have been proposed. The simplest ones are the seminal works that directly probed the statistical interdependence (e.g., Pearson correlation) between separately defined SC and FC measures (Andrews-Hanna et al., 2007; Hagmann et al., 2008; Honey et al., 2009; Supekar et al., 2010; Horn et al., 2014). Limited by the bivariate and summarizing nature of this analysis, the effect is capturing only a general trend of correlation.

In order to directly capture white matter structures that connect temporally coherent areas, several studies initially compute FC and specify implicated regions of interests (ROI) as a seed for estimating fiber streamlines (Greicius et al., 2009; van den Heuvel et al., 2009; Chamberland et al., 2015). Most of these works were specifically directed to the analysis of the default mode network (DMN), a set of brain regions that are known to be more engaged during rest (Greicius et al., 2003). In contrast to extracting SC from FC priors, a number of studies have attempted to reproduce brain activity from predefined structural connectomes through numerical simulations (Galán, 2008; Honey et al., 2007; Deco et al., 2011, 2012, 2013; Goni et al., 2014).

Studies that extract SC from FC or *vice versa* are mostly hypothesis-driven and entail many explicit assumptions (see (Damoiseaux and Greicius, 2009; Zhu et al., 2014) for early reviews). To understand how distributed patterns of functional activity arise from a fixed underlying structure, a need for research methodologies that are observer-independent and data-driven is of utmost importance. A common approach for data-driven methods is based on blind-decomposition techniques. By combining diffusion anisotropy (e.g., fractional anisotropy, axial and radial diffusivities) and classical

* Corresponding author. Institute of Bioengineering, École Polytechnique Fédérale de Lausanne, Geneva, 1202, Switzerland.
E-mail address: anjali.tarun@epfl.ch (A. Tarun).

<https://doi.org/10.1016/j.neuroimage.2020.116718>

Received 11 November 2019; Received in revised form 7 February 2020; Accepted 5 March 2020

Available online 14 March 2020

1053-8119/© 2020 The Authors. Published by Elsevier Inc. This is an open access article under the CC BY-NC-ND license (<http://creativecommons.org/licenses/by-nc-nd/4.0/>).

FC to build a joint SC-FC measure (Sui et al., 2013, 2015), structural and functional alterations in healthy and clinical populations are extracted using multimodal canonical correlation analysis and joint independent component analysis (ICA) (Amico and Goñi, 2018). On the same line, using ICA, concurrent white matter (WM) bundles and gray matter (GM) networks from a tractography-based data matrix have been proposed (O’Muircheartaigh and Jbabdi, 2018). Also using tractography, Calamante and colleagues (Calamante et al., 2017) introduced the concept of track-weighted dynamic FC (TW-dFC), where as a first step, WM streamlines from two structurally connected voxel endpoints are obtained. Then, these streamlines are weighted according to the FC at their endpoints. To render the approach dynamic, FC measures were computed over a sliding-window whose length is arbitrarily chosen. TW-dFC then produces a set of four-dimensional volumes showing the averaged FC between corresponding streamline endpoints onto the WM at the temporal resolution of the window used. While several studies have made considerable progress in linking structure and function, not only with fMRI but also with other imaging modalities such as electroencephalography (EEG) and magnetoencephalography (MEG) (Deslauriers-Gauthier et al., 2019; Fukushima et al., 2015), none of these methods jointly and simultaneously integrates functional and diffusion data into a single integrated framework, which allows the natural emergence of full-brain spatial patterns that cover both the WM and the GM.

Lately, to further transcend our current understanding of structure-function relationships, attention has been set on studying SC and FC through the lens of more technical frameworks borrowed from other research fields, such as propagator-based methods (Robinson, 2012; Robinson et al., 2016; Atasoy et al., 2016), and control network theoretical tools (Gu et al., 2015). Graph signal processing (GSP) for neuroimaging is another emerging field (Huang et al., 2018a), where initially, a graph is defined by identifying regions in GM as nodes, and the strength of their SC through WM as edge weights (e.g., number of streamlines connecting GM regions). Functional data are then defined atop the graph and are interpreted as time-dependent graph signals, on which connectome-informed signal processing operations can be performed. This framework incorporates connectivity through the WM, but only as SC between pairs of GM regions (i.e., WM regions are not explicitly defined as nodes).

In this work, we advance the GSP concept by extending the existing approach from region-wise analysis to a high-resolution (i.e., 850,000 voxels) voxel-level perspective. This translates to modeling the WM explicitly as nodes of the brain graph for which local connectivity is known from DW-MRI. We then define the blood-oxygenation level-dependent (BOLD) time-series from resting-state fMRI as dynamic signals residing on the nodes of the brain graph. By generalizing principles of classical signal processing in regular domains (Buades et al., 2010; Rudin et al., 1992; Chambolle, 2004; Candès et al., 2006) to irregular graphs (Shuman et al., 2013; Chen et al., 2015), we interpolate functional signals, measured on the GM, into the WM, using a whole-brain voxel-wise connectome to guide the process. This allows relating measures of brain activity on the GM with their mediation through WM; i.e., how particular patterns of brain activity jointly rely on an ensemble of WM pathways. We then apply the WM interpolation on all volumes of resting-state data, thereby generating a set of 4D-volumes on which conventional static and dynamic FC tools can be applied. Using the posterior cingulate cortex (PCC), a well-known subcomponent of the DMN, as a seed region, we retrieved new structure-function networks that extend the well-known GM-limited DMN pattern to include the WM. The functional relevance of these structure-function networks is further validated through investigations of their relation to task fMRI. Our results illustrate the structural mechanism for the dynamic switching between task-positive and -negative subsystems of the DMN in different phases of working memory and relational task paradigms.

2. Materials and methods

2.1. Data

We used a total of 51 subjects obtained from the publicly available Human Connectome Project dataset (HCP 1200 release), WU-Minn Consortium. Preprocessed diffusion MRI, original functional MRI, and anatomical data are downloaded following a random subject selection scheme while maintaining a uniform demographic distribution (male and female, ages 22–50). MRI acquisition protocols of the HCP and preprocessing guidelines for diffusion MRI are fully described and discussed elsewhere (Glasser et al., 2013). On the other hand, fMRI data were acquired using Gradient-echo EPI sequence (repetition time [TR]/echo time [TE]/flip angle = 720 ms/33.1 ms/52 deg). Following the standard preprocessing protocol (Van Dijk et al., 2010), four sessions of resting-state fMRI scans (1200 volumes each session, giving a total of 4800 volumes per subject) were realigned to their mean images. The results were then registered and resampled onto the diffusion data using rigid-body registration (SPM12, <https://www.fil.ion.ucl.ac.uk>). The registered images were de-trended (i.e., constant, linear) and smoothed using a Gaussian kernel (FWHM = 6 mm). The first 10 frames were removed to achieve steady-state magnetization of the fMRI data. Meanwhile, the diffusion data were processed using DSI Studio (<http://dsi-studio.labsolver.org>) to estimate the orientation density functions (ODFs) associated with individual voxels across the brain. T1 images were downloaded from the HCP in a readily aligned format corresponding to the diffusion subject space. Individual tissue maps (WM, GM, and cerebrospinal fluid (CSF)) were then segmented from the T1 image using SPM12. The GM probability maps outputted from the segmentation algorithm were thresholded at 0.3 and were used to mask GM voxels.

2.2. Building the voxel-wise brain grid

Similar to classical brain graphs, we define our grid as $\mathcal{G} := (\mathcal{V}, \mathbf{A})$, where $\mathcal{V} = \{1, 2, 3, \dots, N\}$ is the set of N nodes representing the brain voxels (i.e., $N = 700 - 900$ thousand), and $\mathbf{A} \in N \times N$ is an adjacency matrix that encodes the likelihood of water molecules to diffuse from their current position to neighboring voxels. We used an ODF-based weighting-scheme on a three-dimensional 26-neighborhood mesh. ODF is an empirical distribution of water diffusion at different orientations introduced to solve fiber-crossing confounds that are typically observed in model-dependent reconstruction techniques from DW-MRI (Tuch et al., 2003). For more details regarding the choice of the signal reconstruction technique and the design of the brain graph, we refer to the Supplementary Methods and (Tarun et al., 2019). The topology of the brain grid is then validated by defining the graph Laplacian matrix in its symmetric normalized form ($\mathbf{L} = \mathbf{I} - \mathbf{D}^{-\frac{1}{2}}\mathbf{A}\mathbf{D}^{-\frac{1}{2}}$), whose eigendecomposition leads to a complete set of orthonormal eigenvectors that span the graph spectral domain with their corresponding real, non-negative eigenvalues. The top 11 eigenfunctions corresponding to the lowest spatial variation are provided in Supplementary Fig. S2.

2.3. Graph signal recovery formulation

The overall goal of this work is to be able to interpolate signals from the GM into the WM based on the structural information encoded in the voxel-wise connectome. To do this, we consider a cost function that includes a least-squares data-fitting term equal to the residual sum of squares (RSS), and an L2 regularization term that takes into account smoothness with respect to the brain grid, given by

$$\tilde{\mathbf{x}} = \arg \min_{\mathbf{x}} \|\mathbf{y} - \mathbf{B}\mathbf{x}\|^2 + \lambda \mathbf{x}^T \mathbf{L} \mathbf{x}, \quad (1)$$

where \mathbf{y} is a vector of length N containing initial BOLD values within GM nodes and zero elsewhere, \mathbf{B} is an indicator matrix that selects the GM

nodes, and λ is the regularization parameter. \mathbf{L} is the symmetric normalized graph Laplacian, which encodes the voxel-level anatomical structure. The cost function balances between (1) minimizing the RSS and retaining the original GM signals, and (2) imposing smoothness with respect to the structure of the graph. The balance between the two is dictated by the choice of regularization parameter λ . The parameter λ was selected by evaluating the cost of the regularization term $\mathbf{x}^T \mathbf{L} \mathbf{x}$ across a sufficiently large range of λ s, specifically, $\lambda = \{1, 2, 3, \dots, 60\}$. This procedure allowed for a subject-dependent and data-driven choice of the regularization parameter. Fig. S3 shows the plot of the evaluation for all 51 subjects considered in this study; the optimal λ were 9(10), 10(39), 11(2), where the values in the parentheses indicate their frequency of occurrence. The solution to Equation (1) gives the interpolated volume for one time-point in the fMRI. The interpolation is then done repeatedly at each time instance (*i.e.*, each volume) in the functional data.

2.4. Static functional connectivity analysis

The output of the graph signal recovery problem is a set of 4D whole-brain functional volumes at a frame-wise resolution. We used the classical method of static FC analysis (*i.e.*, Pearson correlation) in the interpolated volumes, wherein the averaged BOLD time-course of an ROI is correlated to the activity profiles of all brain voxels to locate temporally coherent areas. We used the PCC, a core region of the DMN, as a seed to observe the joint structural-functional patterns associated with it. This is done to each of the four sessions of resting-state (RS) fMRI sequences per subject, and the corresponding Fisher Z-transformed correlations were averaged across the group.

2.5. Temporal decomposition of DMN-related co-activation patterns

Next, we extended the analysis from static to dynamic FC perspective, using the so-called co-activation pattern (CAP) analysis (Liu and Duyn, 2013). We used the PCC to extract time-varying structural mediation of functional cross-talks implicated with the DMN. To obtain the CAPs, we performed a two-step temporal decomposition: (1) subject-level clustering and (2) group-level matching. For the first part, the top 15% significant frames corresponding to the PCC are extracted in each of the four sessions of resting-state scan from the HCP. Significant volumes that survived the thresholding are concatenated together in each subject. The choice of the threshold is motivated by finding the optimal level of similarity between averaged significant PCC volumes at different thresholds to that of the PCC-seed connectivity outcome (see Supplementary Fig. S4(A)). These significant volumes are then decomposed into multiple co-activation maps by running the k-means clustering algorithm which groups and averages together those with spatially similar frames. The optimal number of clusters was determined using consensus clustering, a resampling based procedure for optimal class discovery (Monti et al., 2003) (see Supplementary Fig. S4(B)). We used cosine as a distance metric and performed 10-folds replicates to obtain the final clustering at the individual level. After obtaining the co-activation maps for each subject, we performed the group-level matching by first transforming all individual maps into a common template (MNI), followed by a one-to-one matching and averaging of the correspondingly similar spatial patterns across subjects.

When doing the clustering at the subject-level, the assignment of CAP indices in one subject does not necessarily correspond to the cluster ordering of another subject. Therefore, when doing the group-level averaging, it is necessary to perform a one-to-one CAP matching and index re-labeling. The one-to-one group-level CAP matching is done using the Hungarian algorithm (Kuhn, 1955), which solves for the optimal pairing that has the most similar spatial combinations as defined by their cosine similarity. The first matching is done on the first two subjects, matching spatially similar CAPs and re-labeling their respective frame indices. Then, the average of the first two is computed, producing a temporary group level CAP from which the third subject is paired with.

This process continues until we reach the last pair of subjects to match. The whole process is repeated again, but this time, the first subject is realigned with the overall average obtained from the first round of group-level CAP matching. Two rounds of subject-to-subject Hungarian matching were done to remove bias on the effect of the first subject.

3. Results

3.1. Recovery of activity in white matter that is compatible with structural connectivity

Signal recovery is a classical task that relates to image denoising (Buades et al., 2010), signal inpainting (Rudin et al., 1992; Chambolle, 2004), and sensing (Candès et al., 2006). Here, we embed the three-dimensional voxel-level grid into a graph where the nodes are voxels, and the edges encode the voxel-wise strength of structural connectivity measured by DW-MRI. Each node has maximally 26 edges and is connected to its closest neighboring voxels. Functional volumes are preprocessed and upsampled to the same resolution as this structural grid. The values from the functional volumes are assigned to each node in the GM, while the remaining nodes, in particular, those in the WM, remain unassigned. The values of the unassigned nodes are then recovered by solving an optimization problem that relies on two assumptions: (i) values in the GM nodes should strongly influence the data fitness (and thus remain reasonably unchanged); (ii) whole-brain signals should maintain smoothness according to the graph structure. The assumption of smoothness with respect to the graph ensures that signals are interpolated according to the brain's structural scaffold. It is important to note, however, that the term *interpolation* does not denote newly generated information, but rather a resulting pattern retrieved by incorporating GM measures with the WM structure.

The overall pipeline is illustrated in Fig. 1(A). For an illustrative frame of resting-state fMRI, we show in Fig. 1(B) an example of the original and the interpolated volumes. Visually, we observe high activity in the PCC and medial prefrontal cortex (mPFC) in the original BOLD signal. After performing the WM interpolation, we recovered additional patterns, such as the cingulum bundle (Lcing) that mediate PCC and mPFC. In addition to major WM bundles that are captured, we also find short-range WM connectivity within the cortical foldings of the GM (Koch et al., 2002). For a quantitative comparison, we used a probabilistic WM atlas provided by Zhang and Arfanakis (2018) to compute the average signal within the cingulum bundle (R/Lcing), and plotted its overall trend throughout the whole timecourse together with the mean signals in the PCC and mPFC. Fig. 1(C) shows that the original PCC-averaged signal bears close similarity (cosine = 0.95) to its interpolated counterpart, a direct consequence of the first constraint imposed in the signal recovery formulation (*i.e.*, retaining the signals within the GM nodes fixed). In contrast, we observe comparatively lower similarities in the mean signals of the interpolated BOLD within the R/Lcing compared to the original BOLD (cosine similarity = 0.34). Meanwhile, PCC, mPFC and the recovered R/Lcing signals all show similar trends (all cosine similarity pairs >0.9), while the original R/Lcing signal displays incoherent activity (cosine similarity with PCC = 0.036). These observations demonstrate that the interpolated functional signals are smooth over the structural brain grid, reflecting in this particular case the existing anatomical pathway (R/Lcing) running from the rostral aspect of the PCC towards the mPFC (Greicius et al., 2009; van den Heuvel et al., 2009).

3.2. PCC-seed connectivity map

In order to capture the joint structural-functional connection of the DMN, we perform a PCC seed-connectivity analysis (Biswal et al., 1995) on the interpolated volumes derived from four sessions of resting-state scans in a population of 51 subjects (244,800 volumes in total). The superior axial slice ($z = 25$) in Fig. 2(A) and (B) shows the PCC and the mPFC, including the bilateral inferior parietal cortex (IPC). In addition to

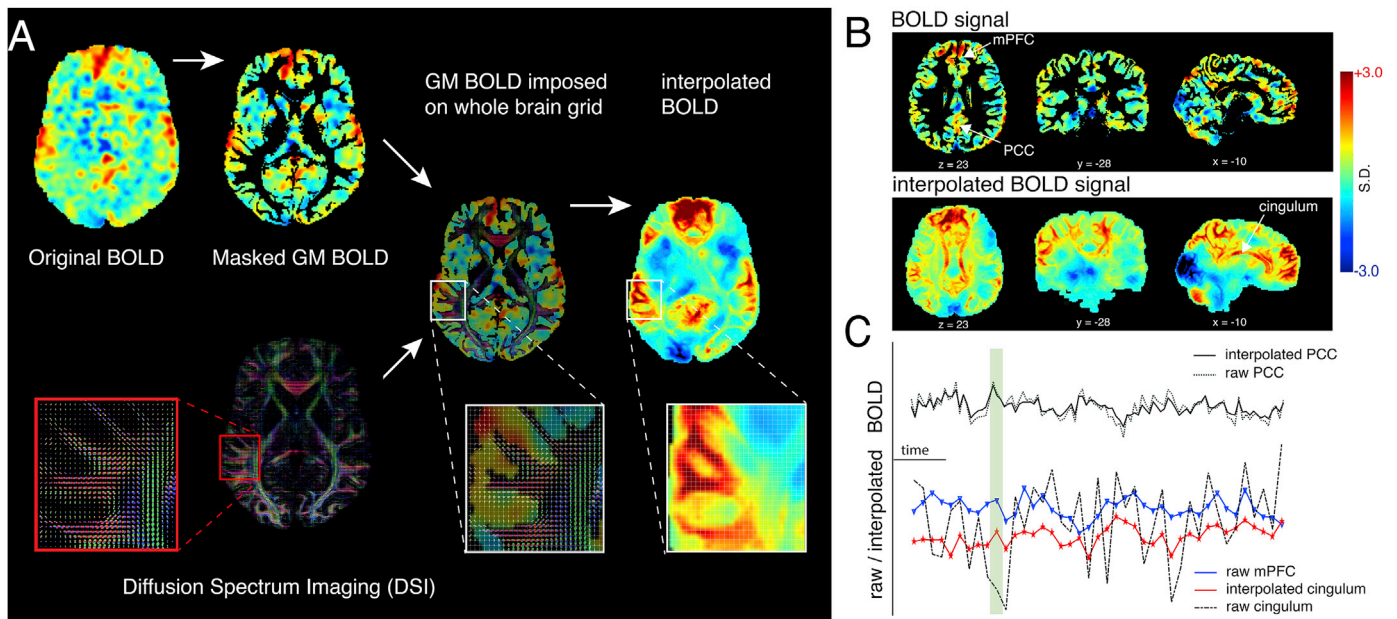


Fig. 1. Workflow of the graph signal recovery framework. (A) GM BOLD signals are extracted from fMRI volumes, one signal per time instance, through masking the volume by the thresholded probabilistic GM map (threshold = 0.3). ODFs associated to all voxels are extracted from the diffusion MRI data. The ODFs are then embedded on a three-dimensional, 26-neighborhood connectivity grid, forming a probabilistic connectome at voxel-level resolution. A signal value can be associated to each voxel on the grid. To initiate signal recovery at each time instance, the associated GM BOLD signal is mapped to the GM voxels within the grid, and the remaining voxels are set to zero. The interpolated BOLD volume is obtained through minimizing a cost function that balances between (1) retaining the GM signal fixed and (2) obtaining a smooth signal over the entire brain grid relative to the underlying structure. (B) Axial, sagittal, and coronal views of a BOLD volume compared to its corresponding interpolated BOLD volume. (C) Original and interpolated BOLD signal time-series of PCC, mPFC and cingulum; the selected time frame in (B) corresponds to the highlighted time point.

the expected GM FC pattern, Fig. 2(B) also shows the distinct WM structures that support the structural connections between these temporally coherent cortical regions. The most prominent connections are the R/Lcing that connect the PCC and the mPFC, the forceps minor (Fminor) that provides intra-connectivity between gyri within the mPFC, and the left and right superior longitudinal fasciculi (R/Lslf) that support the long-range connection between the IPC, and the posterior and frontal regions. Interestingly, we also find the two-sided corticospinal tracts (R/Lcst) that traverse the brainstem all the way to the motor cortex, the genu of the corpus callosum connecting the two hemispheres, as well as the bilateral hippocampal cingulum (R/Lcing2) that exit the caudal aspect of the PCC and continue towards the medial temporal lobe (MTL).

3.3. Structural mediation of dynamic functional connectivity

The axial, sagittal, and coronal slices shown in Fig. 1(B) come from a volume corresponding to a time point with significant activity in the PCC (green shade, Fig. 1(C)). A particular limitation of the PCC-seed connectivity is the inherent static assumption of FC. It has been suggested that the relevant information about RS FC can be condensed into events or short periods of time (e.g., where fMRI timecourses exceed a chosen threshold) (Tagliazucchi et al., 2012). In line with this idea, FC obtained from the conventional seed-correlation analysis has been shown to be approximated by averaging all frames for which the seed has high activity (Liu and Duyn, 2013). This congregation of significantly active frames can then be temporally decomposed into several distinct and meaningful co-activation patterns (CAPs). We applied the CAPs analysis in all interpolated fMRI volumes on each subject. For each session, we determined the significant frames corresponding to the top 15% of the PCC. We then combined all significant volumes on each subject and decomposed them into eight PCC-related CAPs. Then, a group-level matching procedure was performed to obtain the final group-level CAPs.

Fig. 3 presents the CAPs obtained from the interpolated volumes, termed *interpolated CAPs* (in-CAPs), as well as the CAPs generated from

the original BOLD signal, denoted GM CAPs. The resulting spatial patterns reveal a set of WM structures unique to each in-CAP. In-CAP 1 is the most frequently occurring and is characterized by many negative ventral regions, in contrast to its highly positive occipital and frontoparietal regions. In-CAP 2 shows similar characteristics, but with much less pronounced activation in the frontal region, as also seen in its weaker Fminor and R/Lcing. In-CAP 3 exhibits very strong activation in the frontal lobe and negative signals in motor and sensory areas. In-CAPs 4, 5, 6 and 7 all bear high resemblance with the PCC-seed connectivity pattern, but vary in their strength of activity in the occipital and frontoparietal regions; these variations are consequently also reflected in Fminor, Fmajor, R/Lcing, R/Lslf, R/Lilf, as well as the bilateral fronto-occipital fasciculus (R/Lifo). In-CAPs 6 and 7 contain highly negative right and left frontoparietal signals, respectively, demonstrating strong hemispherical asymmetry in their activation patterns. Finally, in-CAP 8 is characterized by positive activation within the ventral brain, specifically in the MTL, but highly negative frontoparietal and somatosensory signals—the implicated WM structures are less pronounced in this in-CAP.

3.4. Spatial and temporal properties of in-CAPs

Whereas GM CAPs reveal instantaneous co-activation of multiple brain regions, in-CAPs complete the structure-function picture through the addition of distinct and functionally relevant WM structures that interpose spatially-distant GM co-activations. To assess the correspondence of the in-CAPs with the DMN subsystems, we computed the average signal within major WM tracts using the probabilistic WM atlas (Zhang and Arfanakis, 2018), and compared them to the main components of the DMN within the GM, as classified by Andrews-Hannah and colleagues (Andrews-Hanna et al., 2010). The probabilistic WM atlas was thresholded to 0.3 to generate the mask (see Supplementary Fig. S4(D) for details of finding the optimal threshold). The signal averaging within WM and GM atlases are computed in both the classical GM CAPs and the inpainted CAPs to be able to compare the two. Fig. 4 reveals good

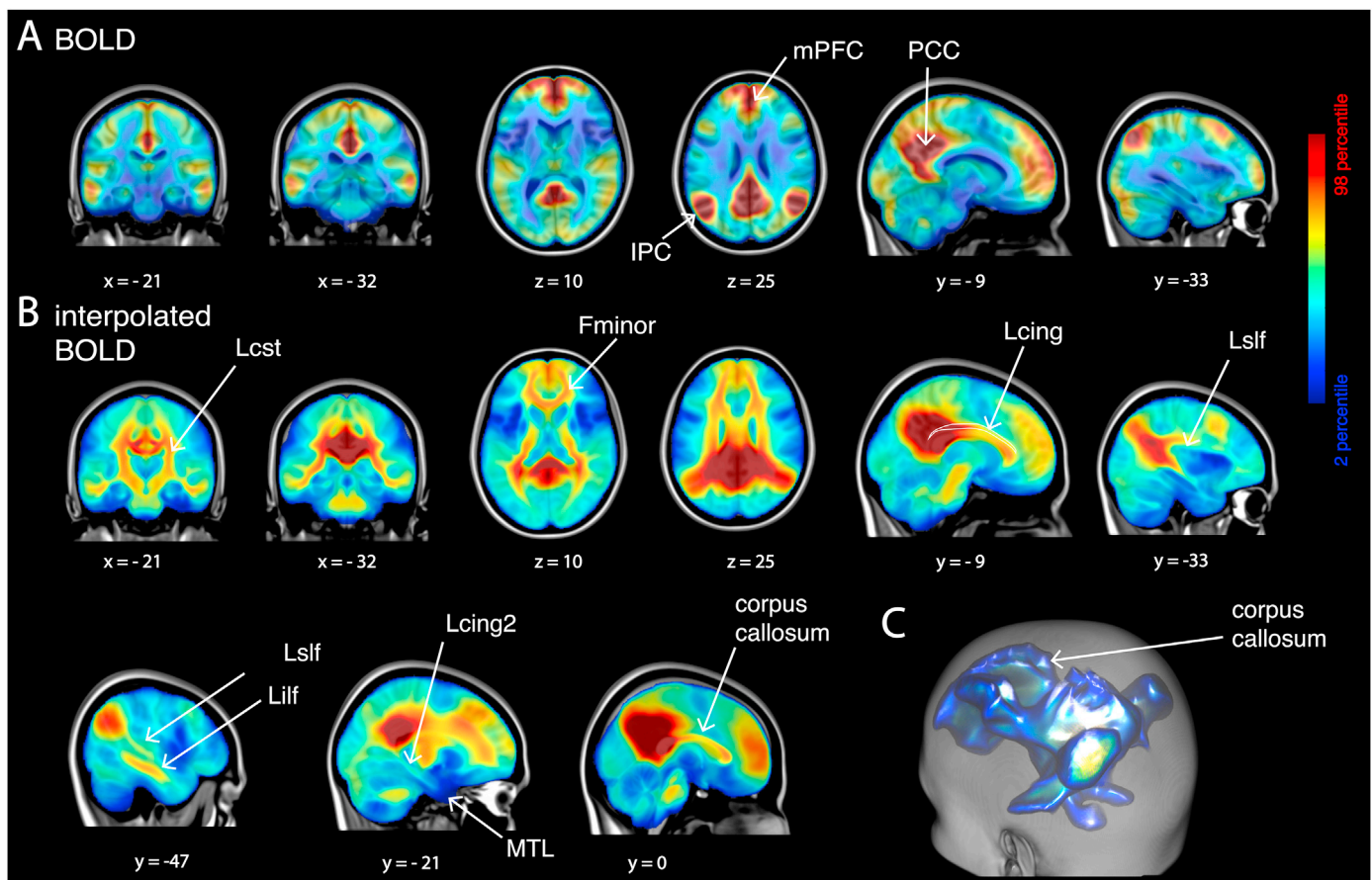


Fig. 2. PCC-seed correlation for the (A) original BOLD volumes and the (B) interpolated volumes, averaged across all subjects. WM bundles connecting temporally-coherent GM regions are uncovered from interpolated volumes. (C) 3D view of the observed WM structure. PCC - posterior cingulate cortex, mPFC - medial prefrontal cortex, Lcst - left cortico-spinal tract, Fminor - forceps minor, Lcing - cingulum, Lslf - left superior longitudinal fasciculus, Lilf - Left inferior longitudinal fasciculus, Lcing2 - hippocampal cingulum.

correspondence in the spatial patterns of GM regions and WM tracts in the inpainted CAPs, especially in terms of activation polarity (with respect to baseline) from the dorsal (positive-valued) to the ventral (negative-valued) side. This is in stark contrast to the spatial patterns of WM tracts in classical GM CAPs showing no accordance with their corresponding GM averages.

Moreover, we further validated the observed tracts in the in-CAPs and PCC seed connectivity based on how much they follow tractography-based results (Greicius et al., 2009; van den Heuvel et al., 2009; Figley et al., 2015). Using predefined ROIs associated to the DMN as seeds, tractography is performed to obtain the WM fiber bundles that connect these regions. We computed the signal averages within the different WM tracts obtained from fMRI-based probabilistic tractography corresponding to the DMN ROIs (Figley et al., 2015). The plot of the signal average is displayed in the Supplementary Fig. S5, side by side with the signal averages computed within the associated DMN ROIs. In general, the signal averages corresponding to the PCC-seed connectivity display positive values in all DMN-related WM tracts, suggesting that the WM interpolation successfully captured tractography-verified WM bundles. On the other hand, the in-CAPs display varied signal averages (i.e., some tracts are positive, some are negative), thereby reflecting the distinct structural-functional organization of the brain at different time points when the PCC is active. These DMN-related WM tracts are all physically connected, but are differentially wired at different time instances.

Next, we assessed the concurrence of the GM CAPs and the in-CAPs by computing the amount of temporal overlap in each CAP. This is done by counting the number of times that a single frame is assigned to a matching in-CAP and GM CAP pair. Fig. 5(A) displays generally matching

frame assignments between the GM CAPs and the in-CAPs, reflecting a strong temporal correspondence between the two CAP types. This finding demonstrates that the addition of the interpolated signals does not interfere with the segregation during the clustering, thereby showcasing the ability of the proposed method in successfully capturing distinct WM structures connecting temporally varying PCC-related networks without compromising information from the original data.

3.5. Relevance of WM interpolated patterns during rest and task

Visual inspection of the spatial averages computed within the WM of all in-CAPs reveals specific patterns that are unique for each in-CAP. In-CAP 8 for instance, displays positive mean signal across all DMN sub-components, and in contrast to all other in-CAPs, also shows a positive bilateral uncinate fasciculus (L/Runc). Previous works have found that activations in both the hippocampus and ventral mPFC during retrieval-mediated learning support novel inference (Zeithamova et al., 2012). We hypothesize that the positive activity of L/Runc in in-CAP 8 reflects its potential role in mediating the coherent activity between the positive temporal poles, hippocampus, and ventral mPFC. To verify this association and to further explore the functional meaning of the obtained in-CAPs, we computed their occurrence probability upon working memory and relational tasks (Fig. 5(B)). To do so, we interpolated signals into the WM as before, extracted frames with high activation in the PCC, and assigned them to their closest in-CAP. We found that although in-CAP 1 is the most recruited at rest, it mostly occurs during task blocks (as opposed to rest intervals). In contrast, in-CAP 8 occurs the least during resting-state, but it is vividly recruited during the rest epochs of

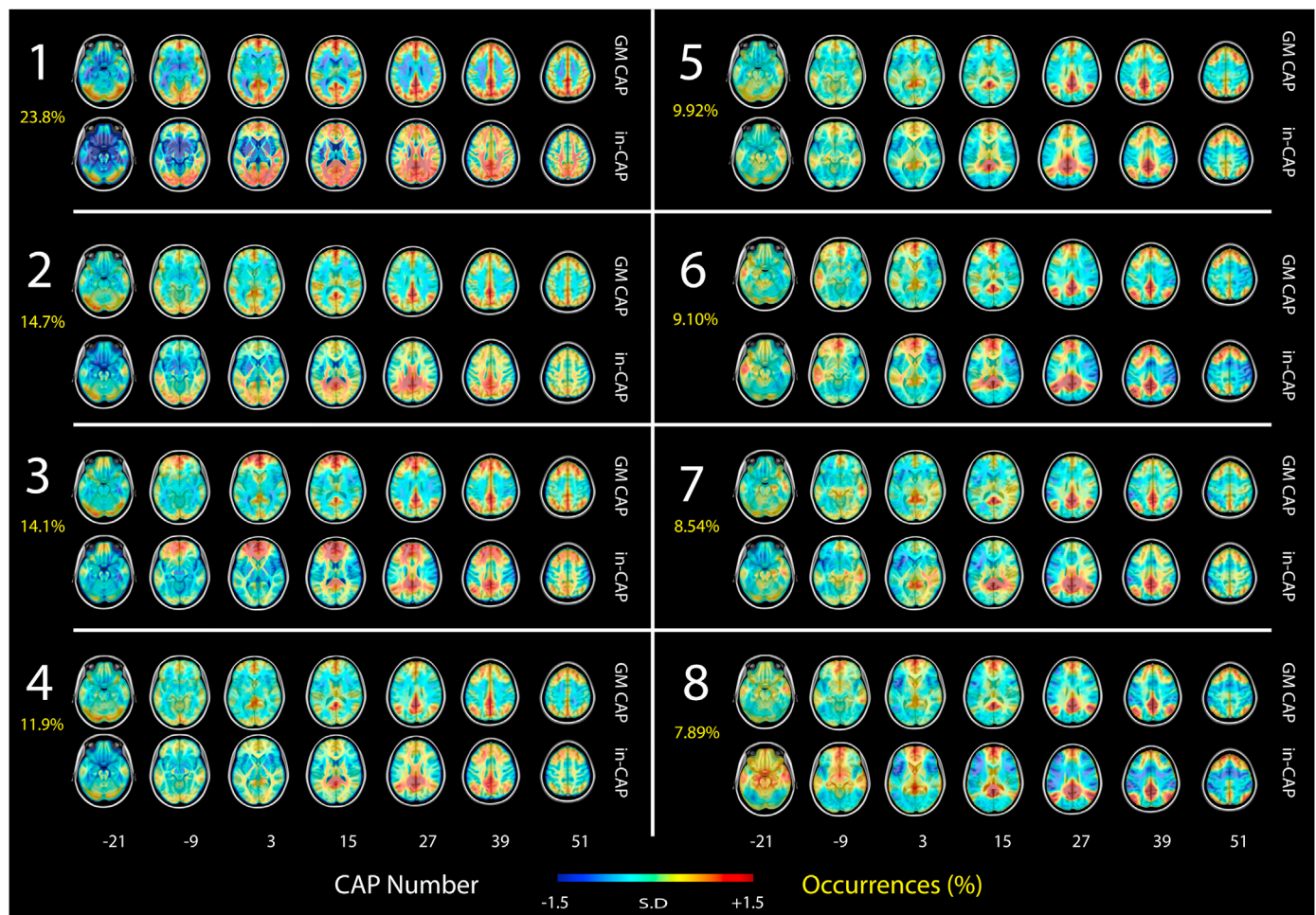


Figure 3. PCC-seed co-activation patterns (CAPs). Eight co-activation maps obtained by temporal decomposition of the top 15% significant frames related to the posterior cingulate cortex (PCC), extracted from (1) the original BOLD volumes (GM CAPs) and (2) interpolated volumes (in-CAPs). The in-CAPs are numbered according to their frequency of occurrence, which is computed by counting the number of frame assignments corresponding to the CAP. Visual inspection of the in-CAPs reveals strong GM similarity with the observed GM CAPs. We found eight distinguishable structure-function networks related to the default mode network (DMN), each of which varies in terms of the observed WM structures that conjoin distinct PCC-coherent GM regions.

the task paradigms. These results are evaluated using a two-factor ANOVA on the occurrences of the different interpolated CAPs during rest and tasks. Results showed highly significant main effects of CAP type and task, as well as the interaction between both, with all corresponding p-values less than 0.0001.

4. Discussion

4.1. General findings

We modeled the brain grid using local, voxel-to-voxel probabilistic connections based on DW-MRI as a large graph onto which brain activity in GM is interpolated into WM. The interpolated brain volumes revealed WM structures that mediate distributed patterns of activity in GM. We explored the neuroscientific relevance of the interpolated volumes by applying conventional static and dynamic FC tools, namely seed-correlation (Biswal et al., 1995) and CAP analysis (Liu and Duyn, 2013), using the PCC as a seed. The resulting in-CAPs unraveled the complexity of recruited WM patterns underlying typically observed GM co-activations (Fig. 3). In-CAPs also showed strong neurophysiological relevance, as they revealed the segregation of the DMN into task-positive and task-negative sub-components (Fig. 5(B)).

4.2. Structure-function relationships of PCC-related networks

Interpolating functional signals measured on GM into the WM has revealed new structural-functional relationships that are akin to the DMN. Fig. 4(D) shows the signal average within WM bundles observed in our PCC seed-correlation map, consistent with the visually observed tracts in Fig. 2. Prominent tracts include the cingulum bundle (R/Lcing), the superior longitudinal fasciculus (R/Lslf), and the forceps minor (Fminor), which are all in close agreement with previous findings of WM structures associated with the DMN (Greicius et al., 2009; van den Heuvel et al., 2009). In addition, the signal averages within DMN-ROI guided tracts (Supplementary Fig. S5) further reflect the success of the signal recovery approach in capturing WM structures that mediate temporally coherent DMN regions. Although seed-correlation analysis is a straightforward measure of FC, it is debased by its transitive nature. The connectivity obtained from this static approach, therefore, summarizes all major WM connections linked to the PCC. On the other hand, CAP analysis can account for time-dependent behavior; thus, the in-CAPs reveal different sets of WM bundles that are characteristic of each of the observed GM CAPs at different time-points.

While it has been established that the DMN anatomically consists of the anterior and posterior midline, the bilateral parietal cortex, pre-frontal cortex, and MTL (Buckner et al., 2008), these regions have been found to functionally dissociate according to the ongoing internal

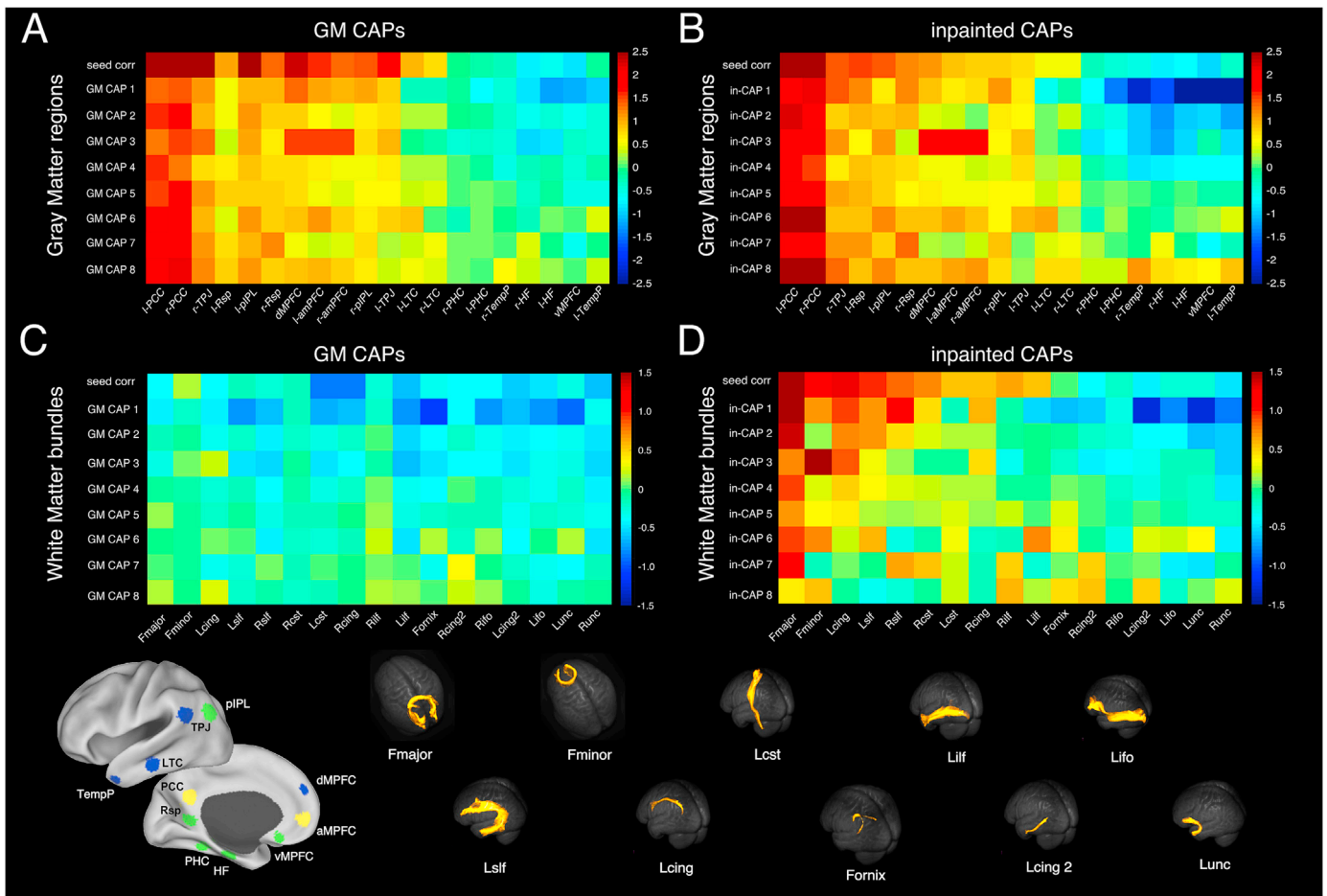


Fig. 4. Spatial characteristics of in-CAPs compared to classical GM CAPs. The overall spatial patterns of the in-CAPs and GM CAPs are explored through spatial averaging of signals within the (A & B) GM sub-components of the DMN (Andrews-Hanna et al., 2010) as well as the (C & D) 17 major WM bundles. A similar spatial trend is observed in the subcomponents of (B) DMN GM in-CAPs and (D) DMN WM in-CAPs, while there is almost no correspondence between the signal averages within (A) DMN GM regions of GM CAPs and the (D) DMN WM bundles of GM CAPs. The arrangement of WM structures and DMN sub-components based on the polarity of the inpainted CAPs with respect to the baseline also shows a concordant pattern of positive-to-negative transition from dorsal-to-ventral regions. Full labels of GM regions and WM bundles are summarized in Supplementary Tables S1 and S2. Figure showing DMN sub-components is adapted with permission from Fig. 1 in ref (Andrews-Hanna et al., 2010).

processes (Andrews-Hanna et al., 2010). We surmise that this functional disintegration is captured by in-CAPs, given that distinct in-CAPs occur in different phases of working and relational memory tasks (Fig. 5(B)). The MTL activates when internal decisions involve constructing a mental scene based on memory (Andrews-Hanna et al., 2010). However, despite being dominantly positive in this region, in-CAP 8 appears to be more active during blocks of rest, and instead, in-CAPs 1 and 2 dominate in periods of task blocks when the stimulus is presented. These findings suggest that in-CAP 8 is a characteristic *task-negative* structure-function network that activates during the maintenance phase (*i.e.*, when subjects are focused on consolidating an observed stimulus). Conversely, in-CAPs 1 and 2 are *task-positive* structure-function networks that are engaged during the encoding and retrieval periods when the external stimulus is presented. Altogether, our results provide new insights into the well-established dichotomy of the human brain (Fox et al., 2005; Greicius et al., 2004), and clearly demonstrate that the DMN and task-positive networks (*e.g.*, attention network, working memory network) are not exclusively expressing opposite activity (Piccoli et al., 2015; Karahanoglu and Van De Ville, 2015).

Arranging the DMN sub-components according to the polarity of their activity in each of the in-CAPs reveals a general trend of positive dorsal areas, such as those observed from PCC to temporal-parietal junction in Fig. 4(B). On the other hand, ventral components (lateral temporal cortex to temporal pole) are more diverse, showing a subtle divide between

more negative (in-CAPs 1–4) versus more positive (in-CAPs 8) ventral default network. The implicated dorsal and ventral WM bundles also show the same trend in Fig. 4(D). In addition, we observe the sagittal slices (Supplementary Fig. S1) of in-CAP 8 to show strong activation in the ventral PCC together with the R/Lcing2. This bundle runs from the caudal aspect of the retrosplenial cortex to the ventrally located hippocampal formation (HF). The bilateral HF, PCC, R/Lcing2, and temporal poles also exhibit positive signals and, therefore, more homogeneous averaged activity. Overall, the above observations highlight the distinctive role of dorsal and ventral parts of the PCC in cognitive control (Karahanoglu and Van De Ville, 2015; Leech et al., 2011). Furthermore, in line with our hypothesis about the role of R/Lunc in memory consolidation, we observe that in-CAP 8 displays positive signal in this particular tract, reflecting its role in mediating coherent activity between the hippocampus and the prefrontal cortex (Squire et al., 2015). Fittingly, it has been found that the deterioration of R/Lunc lowers working-relational memory performance (Hanlon et al., 2012).

4.3. Methodological perspectives

The overall aim of the introduced signal recovery framework is to extract WM structures that mediate the interaction of temporally coherent cortical regions. Several methods that have attempted to achieve the same goal have been proposed over the past years. The most

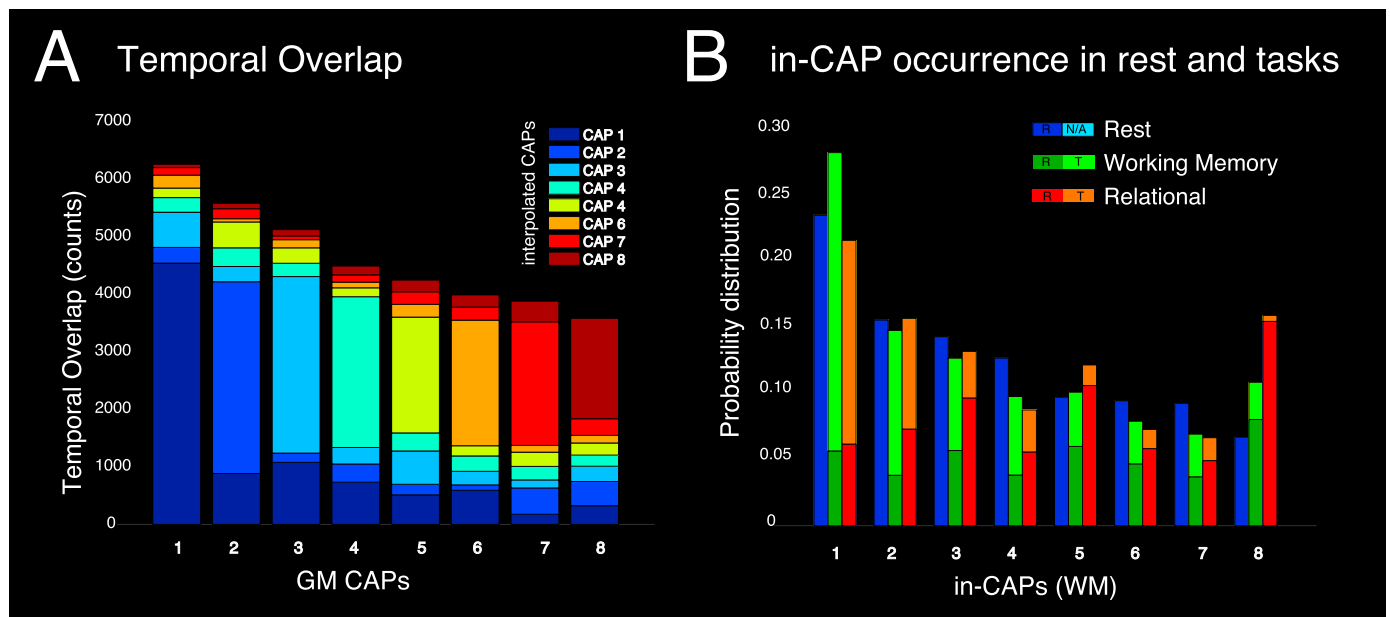


Fig. 5. Temporal characteristics of in-CAPs and their relevance to rest and tasks. (A) Temporal overlap between the interpolated CAPs and the GM CAPs; disregarding the color-code, the height of each bar represents the number of frames that were identified to belong to either of the eight GM CAPs. The sub-bands within each bar show the distribution of the frames linked to a particular GM CAP when classified based on in-CAPs. (B) The probability of occurrence of in-CAPs in resting-state, working memory, and relational tasks. Each bar in the plot corresponds to the probability of that particular in-CAP to appear in the top 15% significant volumes of rest and task scans. The stack of colors denotes the proportion of frames that occur during blocks of rest (R) when there is no stimulus presented, and during blocks of task (T) in which subjects are expected to perform memory or relational tests. Results were verified using two-factor ANOVA (main effects of CAP type and task, and interaction between both), with all p-values less than 0.0001.

straightforward approach is fMRI-guided tractography, where cortical regions corresponding to well-known functional networks are used as seeds to estimate streamlines coming from one ROI to another (Figley et al., 2015; Friman et al., 2006). One obvious limitation of this approach is the need for a two-step procedure, wherein as a first step, ROIs are extracted from functional data, then tractography is launched to recover the streamlines that connect pre-selected regions. In our approach, we go beyond a combined analysis (Zhu et al., 2014) of functional and diffusion MRI, and instead jointly model the two modalities into a single integrated framework that enables the recovery of structure-function patterns which are fully data-driven and observer-independent. Previous works have also introduced a fusion of fMRI and diffusion MRI in a data-driven manner by relying on blind-decomposition techniques (e.g., ICA) and the use of diffusion anisotropy measures to approximate SC (Sui et al., 2013, 2015). However, measures of diffusion anisotropy are unable to resolve crossing fibers as they are extracted from low-order diffusion tensor models, making their interpretation misleading and prone to erroneous conclusions (Wheeler-Kingshott and Cercignani, 2009). Alternatively, a more common approach in defining SC is to count the number of fibers obtained using tractography algorithms (O’Muircheartaigh and Jbabdi, 2018). SC and FC measures can then be combined together into a huge data matrix that is decomposed into independent hybrid structure-function components (Amico and Goñi, 2018). Nevertheless, ICA’s principal assumption of spatial independence leads to components that have low spatial similarity. The high susceptibility of tractography algorithms in generating false positives (Maier-Hein et al., 2017) also warrants caution in interpreting tractography-based results. In contrast, our approach does not rely on tractography, thereby not only bypassing the complicated task of parameter optimization for extracting WM tracts but also not requiring a parcellation scheme to define ROIs. Our framework keeps the analysis close to the DW-MRI data by working directly with local reconstructions of orientation distribution functions, which are consequently encoded, both in direction and magnitude, to build the brain graph. Overall, we believe that our method offers a more

elegant solution to recover WM structures that mediate FC regions, and at the same time, reduces the computational load compared to conventional tractography approaches.

Furthermore, it is worth noting that despite the superficial similarity, there are fundamental differences between our approach and that of the TW-dFC (Calamante et al., 2017). Specifically, both approaches attempt to give a measure of FC into the WM using GM as a constraint. Although TW-dFC jointly fuses fMRI and diffusion MRI, the approach still relies on two successive uses of classical methods (i.e., tractography and sliding-window FC), while our work introduces an entirely new concept where recovery of mediation by SC is incorporating the FC itself in a consolidated framework; i.e., the complete pattern of brain activity in GM is constraining the recovery of WM patterns. In addition, our method works at the single-frame level and does not require to choose a temporal window to render the approach dynamic. It is therefore noteworthy to reiterate that the frame-wise analysis using the CAPs was made possible by the fact that the mediation of GM activation is done for each frame. As such, we make use of the maximal temporal resolution of the functional data, which is a characteristic strength of the introduced method that is not yet overcome by tractography-based methods for jointly integrating FC and SC (Amico and Goñi, 2018; O’Muircheartaigh and Jbabdi, 2018; Calamante et al., 2017). This advantage also translates to easier standardization of results across groups, as classical methods of spatial normalization can be applied in the interpolated volumes in the same manner that is done in original fMRI.

4.4. New research avenues for structure-function studies

GSP approaches as applied to functional neuroimaging rely on a *graph shift operator* (typically the Laplacian or the adjacency matrix) that encodes the brain’s anatomical information. Its eigendecomposition produces an orthogonal set of eigenvectors, termed *eigenmodes*, some of which are reminiscent of well-established functional networks (Atasoy et al., 2016; Abdelnour et al., 2018) and are useful in effectively

estimating the strength of inter-hemispheric interactions in the brain (Robinson et al., 2016). Moreover, efficient anatomically-informed decompositions of fMRI data using a tractography-based structural connectome (Atasoy et al., 2016), as well as topology encoding GM graphs (Behjat et al., 2015) have been proposed. Brain eigenmodes can be viewed as basic building blocks of increasing spatial variation along the structural brain graph, akin to sinusoids in classical Fourier analysis. Here, we extend the traditionally region-level eigenmodes (defined on a limited subset of GM nodes) to a whole-brain (GM and WM), voxel resolution setting (see Supplementary Fig. S2), thus enabling to reconstruct structure-function networks at an unparalleled spatial resolution. As an increasing number of operations are generalized from classical signal processing to the graph setting (Huang et al., 2018a; Shuman et al., 2013; Wang et al., 2017; Becker et al., 2018), promising avenues arise to explore the many facets of brain structure and function.

We therefore foresee two direct avenues for future research. The first avenue aims on leveraging the proposed interpolated fMRI data. The interpolated volumes entail additional informative voxels that extend beyond the GM, which is in particular interesting in light of the limitations and skepticisms in interpreting WM BOLD data (Logothetis and Wandell, 2004; Gawryluk et al., 2014). Previous works have demonstrated the possibility to capture functionally relevant information from the WM BOLD (Peer et al., 2017; Ding et al., 2018; Huang et al., 2018b), despite the well-established findings on the differences of hemodynamic responses in GM and WM (Fraser et al., 2012; Li et al., 2019). At its current form, we interpolate functional signals into the WM as solely constrained by the functional signals from the GM. Alternatively, one may rather consider combining signal interpolation with signal recovery of weak signals in the WM. In our current application, the goal is to observe WM pathways that support distributed patterns of FC in GM, and not on the functional organization of WM itself. The interpolated volumes can then be readily explored using existing tools for dynamic FC analyses (Prete et al., 2017), such as sliding-window correlation, ICA (Beckmann et al., 2005) and principal component analysis (Leonardi et al., 2013), to probe functional brain dynamics at a much larger scale.

The second foreseen research direction is to exploit the proposed anatomically-informed brain grid to implement novel GSP operations on fMRI data. High-resolution eigenmodes enable a spectral graph-based analysis of task-based and resting-state fMRI data at an unprecedented level of detail, and across the whole brain, in contrast to the conventional region-wise analysis, which is typically also limited to the cortical layer. Anatomically-informed spectral graph decomposition of fMRI data using these high-resolution brain eigenmodes is anticipated to open up new perspectives on the brain's functional organization not only within GM but also WM. As a case in point, FC has often been associated to Euclidean distance (Ercsey-Ravasz et al., 2013; Alexander-Bloch et al., 2013); thanks to our framework, the notion of distance becomes more meaningfully defined in terms of the spectral representation of functional signals (Medaglia et al., 2018; Prete and Van De Ville, 2019), enabling a deepened understanding of the roles of short- and long-range connectivity in improving the efficiency of inter-areal brain communication (Betz et al., 2018).

4.5. Technical limitations

While it is true that our approach bypasses the use of tractography algorithms in visualizing WM tracts that support coherent GM activations, our framework is still heavily reliant on the estimation of the orientation density functions. Consequently, our approach is highly dependent on the quality of the diffusion data, as in any other case of DW-MRI studies. We also point out that because we interpolate signals into the WM based on the signals from GM, any discrepancy that is associated with the GM BOLD will likely influence the results of the interpolation. Furthermore, we believe that although jointly integrating functional and diffusion MRI offers several benefits, a potential disadvantage can arise when there is a need to disentangle the effect of the two. This is

particularly true when the approach is applied to clinical populations that are hindered by complex mixes of structural and functional alterations, such as in Multiple Sclerosis patients (Giorgio et al., 2017). In such cases, depending on the hypothesis that can be drawn from the initial results of the inpainting, a detailed case to case analysis is advised. For instance, one may perform a null comparison test, such as contrasting the WM interpolation of a healthy control data to a functionally impaired patient, both of which are interpolated over a structurally deficient brain grid.

5. Conclusion

This study presents a new framework for studying structure-function relationship that has several key advantages. The interpolation of fMRI activity into the white matter enables observing key WM structures that link interacting GM regions at the single-frame resolution. We believe that the introduction of highly-resolved human brain eigenmodes can (i) shift the existing trend of constructing region-wise connectomes to that of voxel-wise connectomes and (ii) expand the use of the GSP repertoire in the context of functional brain imaging. More importantly, we anticipate the proposed joint structure-function characterization to offer unprecedented benefits for the study of clinical populations, particularly those born with structural deficits but preserved functional efficiency, such as in patients with agenesis of the corpus callosum (Tovar-Moll et al., 2014; Owen et al., 2013).

Declaration of competing interest

The authors declare that they have no competing financial interests.

CRediT authorship contribution statement

Anjali Tarun: Conceptualization, Methodology, Software, Validation, Formal analysis, Data curation, Writing - original draft, Writing - review & editing. **Hamid Behjat:** Methodology, Writing - review & editing. **Thomas Bolton:** Writing - review & editing. **David Abramian:** Methodology, Writing - review & editing. **Dimitri Van De Ville:** Conceptualization, Methodology, Writing - review & editing, Supervision.

Acknowledgements

A.T. is supported by the Swiss National Science Foundation under the Project Grant 205321-163376.

Appendix A. Supplementary data

Supplementary data to this article can be found online at <https://doi.org/10.1016/j.neuroimage.2020.116718>.

References

- Abdelnour, F., Dayan, M., Devinsky, O., Thesen, T., Raj, A., 2018. Functional brain connectivity is predictable from anatomic network's Laplacian eigen-structure. *NeuroImage* 172, 728–739. <https://doi.org/10.1016/j.neuroimage.2018.02.016>.
- Alexander-Bloch, A.F., Vértes, P.E., Stidd, R., Lalonde, F., Clasen, L., Rapoport, J., Giedd, J., Bullmore, E., Gogtay, N., 2013. The anatomical distance of functional connections predicts brain network topology in health and schizophrenia. *Cerebr. Cortex* 23, 127–138. <https://doi.org/10.1093/cercor/bhr388>.
- Amico, E., Goñi, J., 2018. Mapping hybrid functional-structural connectivity traits in the human connectome. *Netw. Neurosci.* 2, 306–322. https://doi.org/10.1162/netn_a_00049.
- Andrews-Hanna, J.R., Snyder, A.Z., Vincent, J.L., Lustig, C., Head, D., Raichle, M.E., Buckner, R.L., 2007. Disruption of large-scale brain systems in advanced aging. *Neuron* 56, 924–935. <https://doi.org/10.1016/j.neuron.2007.10.038>.
- Andrews-Hanna, J.R., Reidler, J.S., Sepulcre, J., Poulin, R., Buckner, R.L., 2010. Functional-Anatomic fractionation of the brain's default network. *Neuron* 65, 550–562. <https://doi.org/10.1016/j.neuron.2010.02.005>.
- Atasoy, S., Donnelly, I., Pearson, J., 2016. Human brain networks function in connectome-specific harmonic waves. *Nat. Commun.* 7, 10340. <https://doi.org/10.1038/ncomms10340>.

- Becker, C.O., Pequito, S., Pappas, G.J., Miller, M.B., Grafton, S.T., Bassett, D.S., Preciado, V.M., et al., 2018. Spectral mapping of brain functional connectivity from diffusion imaging. *Sci. Rep.* 8, 1411. <https://doi.org/10.1038/s41598-017-18769-x>.
- Beckmann, C.F., DeLuca, M., Devlin, J.T., Smith, S.M., 2005. Investigations into resting-state connectivity using independent component analysis. *Phil. Trans. Biol. Sci.* 360, 1001–1013. <https://doi.org/10.1098/rstb.2005.1634>.
- Behjat, H., Leonardi, N., Sörmo, L., Van De Ville, D., 2015. Anatomically-adapted graph wavelets for improved group-level fMRI activation mapping. *Neuroimage* 123, 185–199. <https://doi.org/10.1016/j.neuroimage.2015.06.010>.
- Betzler, R.F., Bassett, D.S., 2018. Specificity and robustness of long-distance connections in weighted, interareal connectomes. *Proc. Natl. Acad. Sci. Unit. States Am.* 115, E4880–E4889. <https://doi.org/10.1073/pnas.1720186115>.
- Biswal, B.F., Yetkin, Z., Haughton, V.M., Hyde, J.S., 1995. Functional connectivity in the motor cortex of resting human brain using echo-planar MRI. *Magn. Reson. Med.* 34, 537–541. <https://doi.org/10.1002/mrm.1910340409>.
- Buades, A., Coll, B., Morel, J.-m., 2010. A review of image denoising algorithms, with a new one. *SIAM J. Multiscale Model. Simul.: A SIAM Interdiscipl. J.* 4, 490–530. URL <https://hal.archives-ouvertes.fr/hal-00271141/document>.
- Buckner, R.L., Andrews-Hanna, J.R., Schacter, D.L., 2008. The brain's default network: anatomy, function, and relevance to disease. *Ann. N. Y. Acad. Sci.* 1124, 1–38. <https://doi.org/10.1196/annals.1440.011>.
- Bullmore, E., Sporns, O., 2009. Complex brain networks: graph theoretical analysis of structural and functional systems. *Nat. Rev. Neurosci.* 10, 186–198. <https://doi.org/10.1038/nrn2575>.
- Calamante, F., Smith, R.E., Liang, X., Zalesky, A., Connelly, A., 2017. Track-weighted dynamic functional connectivity (TW-dFC): a new method to study time-resolved functional connectivity. *Brain Struct. Funct.* 222, 3761–3774. <https://doi.org/10.1007/s00429-017-1431-1>.
- Candès, E.J., Romberg, J.K., Tao, T., 2006. Stable signal recovery from incomplete and inaccurate measurements. *Commun. Pure Appl. Math.* 59, 1207–1223. <https://doi.org/10.1002/cpa.20124.0503066>.
- Chamberland, M., Bernier, M., Fortin, D., Whittingstall, K., Descoteaux, M., 2015. 3D interactive tractography-informed resting-state fMRI connectivity. *Front. Neurosci.* 9, 1–15. <https://doi.org/10.3389/fnins.2015.00275>.
- Chambolle, A., 2004. An algorithm for total variation minimization and applications. *J. Math. Imag. Vis.* 20, 89–97. <https://doi.org/10.1023/B:JMIV.0000011321.19549.88>.
- Chen, S., Sandryhaila, A., Moura, J.M.F., Kovacevic, J., 2015. Signal recovery on graphs: variation minimization. *IEEE Trans. Signal Process.* 63, 4609–4624. <https://doi.org/10.1109/TSP.2015.2441042>.
- Damoiseaux, J.S., Greicius, M.D., 2009. Greater than the sum of its parts: a review of studies combining structural connectivity and resting-state functional connectivity. *Brain Struct. Funct.* 213, 525–533. <https://doi.org/10.1007/s00429-009-0208-6>.
- Deco, G., Jirsa, V.K., McIntosh, A.R., 2011. Emerging concepts for the dynamical organization of resting-state activity in the brain. *Nat. Rev. Neurosci.* 12, 43–56. <https://doi.org/10.1038/nrn2961>.
- Deco, G., Senden, M., Jirsa, V., 2012. How anatomy shapes dynamics: a semi-analytical study of the brain at rest by a simple spin model. *Front. Comput. Neurosci.* 6, 1–7. <https://doi.org/10.3389/fncom.2012.00068>.
- Deco, G., Ponce-Alvarez, A., Mantini, D., Romani, G.L., Hagmann, P., Corbetta, M., 2013. Resting-state functional connectivity emerges from structurally and dynamically shaped slow linear fluctuations. *J. Neurosci.* 33, 11239–11252. <https://doi.org/10.1523/JNEUROSCI.1091-13.2013>.
- Deslauriers-Gauthier, S., Lina, J., Butler, R., Whittingstall, K., Gilbert, G., Bernier, P., Deriche, R., Descoteaux, M., 2019. White matter information flow mapping from diffusion MRI and EEG. *Neuroimage* 201, 116017. <https://doi.org/10.1016/j.neuroimage.2019.116017>.
- Ding, Z., Huang, Y., Bailey, S., Gao, Y., Cutting, L., Rogers, B., Newton, A., Gore, J., 2018. Detection of synchronous brain activity in white matter tracts at rest and under functional loading. *Proc. Natl. Acad. Sci. Unit. States Am.* 115, 595–600. <https://doi.org/10.1073/pnas.1711567115>.
- Ercsey-Ravasz, M., Markov, N., Lamy, C., Van Essen, D., Knoblauch, K., Toroczkai, Z., Kennedy, H., 2013. A predictive network model of cerebral cortical connectivity based on a distance rule. *Neuron* 80, 184–197. <https://doi.org/10.1016/j.neuron.2013.07.036>.
- Figley, T.D., Bhullar, N., Courtney, S.M., Figley, C.R., 2015. Probabilistic atlases of default mode, executive control and salience network white matter tracts: an fMRI-guided diffusion tensor imaging and tractography study. *Front. Hum. Neurosci.* 9, 1–20. <https://doi.org/10.3389/fnhum.2015.00585>.
- Fox, M.D., Snyder, A.Z., Vincent, J.L., Corbetta, M., Van Essen, D.C., Raichle, M.E., 2005. The human brain is intrinsically organized into dynamic, anticorrelated functional networks. *Proc. Natl. Acad. Sci. Unit. States Am.* 102, 9673–9678. <https://doi.org/10.1073/pnas.0504136102>.
- Fraser, L.M., Stevens, M., Beyea, S.D., D'Arcy, R.C.N., 2012. White versus gray matter: fMRI hemodynamic responses show similar characteristics, but differ in peak amplitude. *BMC Neurosci.* 13, 91. <https://doi.org/10.1186/1471-2202-13-91>.
- Friman, O., Farneback, G., Westin, C.-F., 2006. A Bayesian approach for stochastic white matter tractography. *IEEE Trans. Med. Imag.* 25, 965–978. <https://doi.org/10.1109/TMI.2006.877093>.
- Friston, K.J., 1994. Functional and effective connectivity in neuroimaging: a synthesis. *Hum. Brain Mapp.* 56–78. <https://doi.org/10.1002/hbm.460020107>.
- Fukushima, M., Yamashita, O., Knösche, T.R., Sato, M.-a., 2015. MEG source reconstruction based on identification of directed source interactions on whole-brain anatomical networks. *Neuroimage* 105, 408–427. <https://doi.org/10.1016/j.neuroimage.2014.09.066>.
- Galán, R.F., 2008. On how network architecture determines the dominant patterns of spontaneous neural activity. *PLoS One* 3, e2148. <https://doi.org/10.1371/journal.pone.0002148>.
- Gawryluk, J.R., Mazerolle, E.L., D'Arcy, R.C.N., 2014. Does functional MRI detect activation in white matter? A review of emerging evidence, issues, and future directions. *Front. Neurosci.* 8, 1–12. <https://doi.org/10.3389/fnins.2014.00239>.
- Giorgio, A., Zhang, J., Stromillo, M., Rossi, F., Battaglini, M., Nichelli, L., Mortilla, M., Portaccio, E., Hakiki, B., Amato, M., De Stefano, N., 2017. Pronounced structural and functional damage in early adult pediatric-onset multiple Sclerosis with No or minimal clinical disability. *Front. Neurol.* 8. <https://doi.org/10.3389/fneur.2017.00608>.
- Glasser, M.F., Sotiropoulos, S.N., Wilson, J.A., Coalson, T.S., Fischl, B., Andersson, J.L., Xu, J., Jbabdi, S., Webster, M., Polimeni, J.R., Van Essen, D.C., Jenkinson, M., 2013. The minimal preprocessing pipelines for the Human Connectome Project. *Neuroimage* 80, 105–124. <https://doi.org/10.1016/j.neuroimage.2013.04.127>.
- Goni, J., van den Heuvel, M.P., Avena-Koenigsberger, A., Velez de Mendizabal, N., Betzel, R.F., Griffa, A., Hagmann, P., Corominas-Murtra, B., Thiran, J.P., Sporns, O., 2014. Resting-brain functional connectivity predicted by analytic measures of network communication. *Proc. Natl. Acad. Sci. Unit. States Am.* 111, 833–838. <https://doi.org/10.1073/pnas.1315529111>.
- Greicius, M.D., Krasnow, B., Reiss, A.L., Menon, V., 2003. Functional connectivity in the resting brain: a network analysis of the default mode hypothesis. *Proc. Natl. Acad. Sci. Unit. States Am.* 100, 253–258. <https://doi.org/10.1073/pnas.0135058100>.
- Greicius, M.D., Srivastava, G., Reiss, A.L., Menon, V., 2004. Default-mode network activity distinguishes Alzheimer's disease from healthy aging: evidence from functional MRI. *Proc. Natl. Acad. Sci. Unit. States Am.* 101, 4637–4642. <https://doi.org/10.1073/pnas.0308627101>.
- Greicius, M.D., Supek, K., Menon, V., Dougherty, R.F., 2009. Resting-state functional connectivity reflects structural connectivity in the default mode network. *Cerebr. Cortex* 19, 72–78. <https://doi.org/10.1093/cercor/bhn059>.
- Gu, S., Pasqualetti, F., Cieslak, M., Telesford, Q.K., Yu, A.B., Kahn, A.E., Medaglia, J.D., Vettel, J.M., Miller, M.B., Grafton, S.T., Bassett, D.S., 2015. Controllability of structural brain networks. *Nat. Commun.* 6, 8414. <https://doi.org/10.1038/ncomms9414>.
- Hagmann, P., Cammoun, L., Gigandet, X., Meuli, R., Honey, C.J., Wedeen, V.J., Sporns, O., 2008. Mapping the structural core of human cerebral cortex. *PLoS Biol.* 6, e159. <https://doi.org/10.1371/journal.pbio.0060159>.
- Hanlon, F.M., Houck, J.M., Klimaj, S.D., Caprihan, A., Mayer, A.R., Weisend, M.P., Bustillo, J.R., Hamilton, D.A., Tesche, C.D., 2012. Frontotemporal anatomical connectivity and working-relational memory performance predict everyday functioning in schizophrenia. *Psychophysiology* 49, 1340–1352. <https://doi.org/10.1111/j.1469-8986.2012.01448.x>.
- Honey, C.J., Kotter, R., Breakspear, M., Sporns, O., 2007. Network structure of cerebral cortex shapes functional connectivity on multiple time scales. *Proc. Natl. Acad. Sci. Unit. States Am.* 104, 10240–10245. <https://doi.org/10.1073/pnas.0701519104>.
- Honey, C.J., Sporns, O., Cammoun, L., Gigandet, X., Thiran, J.P., Meuli, R., Hagmann, P., 2009. Predicting human resting-state functional connectivity from structural connectivity. *Proc. Natl. Acad. Sci. Unit. States Am.* 106, 2035–2040. <https://doi.org/10.1073/pnas.0811168106>.
- Horn, A., Ostwald, D., Reisert, M., Blankenburg, F., 2014. The structural-functional connectome and the default mode network of the human brain. *Neuroimage* 102, 142–151. <https://doi.org/10.1016/j.neuroimage.2013.09.069>.
- Huang, Y., Bailey, S.K., Wang, P., Cutting, L.E., Gore, J.C., Ding, Z., 2018. Voxel-wise detection of functional networks in white matter. *Neuroimage* 183, 544–552. <https://doi.org/10.1016/j.neuroimage.2018.08.049>.
- Huang, W., Bolton, T.A.W., Medaglia, J.D., Bassett, D.S., Ribeiro, A., Van De Ville, D., 2018. A graph signal processing perspective on functional brain imaging. *Proc. IEEE* 106, 868–885. <https://doi.org/10.1109/JPROC.2018.2798928>.
- Karahanoglu, F.I., Van De Ville, D., 2015. Transient brain activity disentangles fMRI resting-state dynamics in terms of spatially and temporally overlapping networks. *Nat. Commun.* 6, 7751. <https://doi.org/10.1038/ncomms8751>.
- Koch, M.A., Norris, D.G., Hund-Georgiadis, M., 2002. An investigation of functional and anatomical connectivity using magnetic resonance imaging. *Neuroimage* 16, 241–250. <https://doi.org/10.1006/nimg.2001.1052>.
- Kuhn, H.W., 1955. The Hungarian method for the assignment problem. *Nav. Res. Logist. Q.* 2, 83–97. <https://doi.org/10.1002/nav.3800020109>.
- Leech, R., Kamourieh, S., Beckmann, C.F., Sharp, D.J., 2011. Fractionating the default mode network: distinct Contributions of the ventral and dorsal posterior cingulate cortex to cognitive control. *J. Neurosci.* 31, 3217–3224. <https://doi.org/10.1523/JNEUROSCI.5626-10.2011>.
- Leonardi, N., Richiardi, J., Gschwind, M., Simioni, S., Annoni, J., Schlupe, M., Vuilleumier, P., Van De Ville, D., 2013. Principal components of functional connectivity: a new approach to study dynamic brain connectivity during rest. *Neuroimage* 83, 937–950. <https://doi.org/10.1016/j.neuroimage.2013.07.019>.
- Li, M., Newton, A.T., Anderson, A.W., Ding, Z., Gore, J.C., 2019. Characterization of the hemodynamic response function in white matter tracts for event-related fMRI. *Nat. Commun.* 10, 1140. <https://doi.org/10.1038/s41467-019-09076-2>.
- Liu, X., Duyn, J.H., 2013. Time-varying functional network information extracted from brief instances of spontaneous brain activity. *Proc. Natl. Acad. Sci. Unit. States Am.* 110, 4392–4397. <https://doi.org/10.1073/pnas.1216856110>.
- Logothetis, N.K., Wandell, B.A., 2004. Interpreting the BOLD signal. *Annu. Rev. Physiol.* 66, 735–769. <https://doi.org/10.1146/annurev.physiol.66.082602.092845>.
- Maier-Hein, K.H., Neher, P.F., Houde, J.C., Côté, M.A., Garryfallides, E., Zhong, J., Chamberland, M., Yeh, F.C., Lin, Y.C., Ji, Q., Reddick, W.E., Glass, J.O., Chen, D.Q., 2017. The challenge of mapping the human connectome based on diffusion tractography. *Nat. Commun.* 8, 1349. <https://doi.org/10.1038/s41467-017-01285-x>.

- Medaglia, J.D., Huang, W., Karuza, E.A., Kelkar, A., Thompson-schill, S.L., Ribeiro, A., Bassett, D.S., 2018. Functional alignment with anatomical networks is associated with cognitive flexibility. *Nat. Hum. Behav.* 2, 156–164. <https://doi.org/10.1038/s41562-017-0260-9>.
- Monti, S., Tamayo, P., Mesirov, J., Golub, T., 2003. Consensus clustering: a resampling-based method for class discovery and visualization of gene expression microarray data. *Mach. Learn.* 52, 91–118. <https://doi.org/10.1023/A:1023949509487>.
- Owen, J.P., Li, Y., Yang, F.G., Shetty, C., Bukshpun, P., Vora, S., Wakahiro, M., Hinkley, L.B.N., Nagarajan, S.S., Sherr, E.H., Mukherjee, P., 2013. Resting-state networks and the functional connectome of the human brain in agenesis of the corpus callosum. *Brain Connect.* 3, 547–562. <https://doi.org/10.1089/brain.2013.0175>.
- O’Muircheartaigh, J., Jbabdi, S., 2018. Concurrent white matter bundles and grey matter networks using independent component analysis. *Neuroimage* 170, 296–306. <https://doi.org/10.1016/j.neuroimage.2017.05.012>.
- Peer, M., Nitzan, M., Bick, A.S., Levin, N., Arzy, S., 2017. Evidence for functional networks within the human brain’s white matter. *J. Neurosci.* 37, 6394–6407. <https://doi.org/10.1523/JNEUROSCI.3872-16.2017>.
- Piccoli, T., Valente, G., Linden, D.E.J., Re, M., Esposito, F., Sack, A.T., Salle, F.D., 2015. The default mode network and the working memory network are not anti-correlated during all phases of a working memory task. *PLoS One* 10, e0123354. <https://doi.org/10.1371/journal.pone.0123354>.
- Preti, M.G., Bolton, T.A., Van De Ville, D., 2019. Decoupling of brain function from structure reveals regional behavioral specialization in humans. *Nat. Commun.* 10, 4747. <https://doi.org/10.1038/s41467-019-12765-7>.
- Preti, M.G., Bolton, T.A., Van De Ville, D., 2017. The dynamic functional connectome: state-of-the-art and perspectives. *Neuroimage* 160, 41–54. <https://doi.org/10.1016/j.neuroimage.2016.12.061>.
- Robinson, P.A., 2012. Interrelating anatomical, effective, and functional brain connectivity using propagators and neural field theory. *Phys. Rev.* 85, 011912. <https://doi.org/10.1103/PhysRevE.85.011912>.
- Robinson, P., Zhao, X., Aquino, K.M., Griffiths, J.D., Sarkar, S., Mehta-Pandjee, G., 2016. Eigenmodes of brain activity: neural field theory predictions and comparison with experiment. *Neuroimage* 142, 79–98. <https://doi.org/10.1016/j.neuroimage.2016.04.050>.
- Rudin, L.L., Osher, S., Fatemi, E., 1992. Nonlinear total variation based noise removal algorithms. *Physica D* 60, 259–268. [https://doi.org/10.1016/0167-2789\(92\)90242-F](https://doi.org/10.1016/0167-2789(92)90242-F).
- Shuman, D.I., Narang, S.K., Frossard, P., Ortega, A., Vandergheynst, P., 2013. The emerging field of signal processing on graphs: extending high-dimensional data analysis to networks and other irregular domains. *IEEE Signal Process. Mag.* 30, 83–98. <https://doi.org/10.1109/MSP.2012.2235192>.
- Squire, L.R., Genzel, L., Wixted, J.T., Morris, R.G., 2015. Memory consolidation. *Cold Spring Harbor Perspect. Biol.* 7, a021766. <https://doi.org/10.1101/cshperspect.a021766>.
- Sui, J., He, H., Pearlson, G.D., Adali, T., Kiehl, K.A., Yu, Q., Clark, V.P., Castro, E., White, T., Mueller, B.A., 2013. Three-way (N-way) fusion of brain imaging data based on mCCA+jICA and its application to discriminating schizophrenia. *Neuroimage* 66, 119–132. <https://doi.org/10.1016/j.neuroimage.2012.10.051Q>.
- Sui, J., Pearlson, G.D., Du, Y., Yu, Q., Jones, T.R., Chen, J., Jiang, T., Bustillo, J., Calhoun, V.D., 2015. In search of multimodal neuroimaging biomarkers of cognitive deficits in schizophrenia. *Biol. Psychiatr.* 78, 794–804. <https://doi.org/10.1016/j.biopsych.2015.02.017Q>.
- Supekar, K., Uddin, L.Q., Prater, K., Amin, H., Greicius, M.D., Menon, V., 2010. Development of functional and structural connectivity within the default mode network in young children. *Neuroimage* 52, 290–301. <https://doi.org/10.1016/j.neuroimage.2010.04.009>.
- Tagliazucchi, E., Balenzuela, P., Fraiman, D., Chialvo, D.R., 2012. Criticality in large-scale brain fMRI dynamics unveiled by a novel point process analysis. *Front. Physiol.* 3, 1–12. <https://doi.org/10.3389/fphys.2012.00015>.
- Tarun, A., Abramian, D., Behjat, H., De Ville, D.V., 2019. Graph spectral analysis of voxel-wise brain graphs from diffusion-weighted MRI. In: 2019 *IEEE 16th International Symposium On Biomedical Imaging (ISBI 2019)*, Isbi. IEEE, pp. 159–163. doi:10.1109/ISBI.2019.8759496.
- Tovar-Moll, F., Monteiro, M., Andrade, J., Bramati, I., Vianna-Barbosa, R., Marins, T., Rodrigues, E., Dantas, N., Behrens, T.E.J., de Oliveira-Souza, R., Moll, J., Lent, R., 2014. Structural and functional brain rewiring clarifies preserved interhemispheric transfer in humans born without the corpus callosum. *Proc. Natl. Acad. Sci. Unit. States Am.* 111, 7843–7848. <https://doi.org/10.1073/pnas.1400806111>.
- Tuch, D.S., Reese, T.G., Wiegell, M.R., Wedeen, Van J., 2003. Diffusion MRI of complex neural architecture. *Neuron* 40, 885–895. [https://doi.org/10.1016/S0896-6273\(03\)00758-X](https://doi.org/10.1016/S0896-6273(03)00758-X).
- van den Heuvel, M.P., Mandl, R.C., Kahn, R.S., Hulshoff Pol, H.E., 2009. Functionally linked resting-state networks reflect the underlying structural connectivity architecture of the human brain. *Hum. Brain Mapp.* 30, 3127–3141. <https://doi.org/10.1002/hbm.20737>.
- Van Dijk, K.R.A., Hedden, T., Venkataraman, A., Evans, K., Lazar, S., Buckner, R., 2010. Intrinsic functional connectivity as a tool for human connectomics: theory, properties, and optimization. *J. Neurophysiol.* 103, 297–321. <https://doi.org/10.1152/jn.00783.2009>.
- Wang, M.B., Owen, J.P., Mukherjee, P., Raj, A., 2017. Brain network eigenmodes provide a robust and compact representation of the structural connectome in health and disease. *PLoS Comput. Biol.* 13, e1005550. <https://doi.org/10.1371/journal.pcbi.1005550>.
- Wheeler-Kingshott, C.A., Cercignani, A.M., 2009. About “axial” and “radial” diffusivities. *Magn. Reson. Med.* 61, 1255–1260. <https://doi.org/10.1002/mrm.21965>.
- Zeithamova, D., Dominick, A.L., Preston, A.R., 2012. Hippocampal and ventral medial prefrontal activation during retrieval-mediated learning supports novel inference. *Neuron* 75, 168–179. <https://doi.org/10.1016/j.neuron.2012.05.010>.
- Zhang, S., Arfanakis, K., 2018. Evaluation of standardized and study-specific diffusion tensor imaging templates of the adult human brain: template characteristics, spatial normalization accuracy, and detection of small inter-group FA differences. *Neuroimage* 172, 40–50. <https://doi.org/10.1016/j.neuroimage.2018.01.046>.
- Zhu, D., Zhang, T., Jiang, X., Hu, X., Chen, H., Yang, N., Lv, J., Han, J., Guo, L., Liu, T., 2014. Fusing DTI and fMRI data: a survey of methods and applications. *Neuroimage* 102, 184–191. <https://doi.org/10.1016/j.neuroimage.2013.09.071Q>.